Nuclear Instruments and Methods in Physics Research A 368 (1996) 345–352

ELSEVIER

NUCLEAR INSTRUMENTS & METHODS IN PHYSICS RESEARCH Section A

Study of the bunch crossing identification at LHC using microstrip gas chambers

F. Angelini[a], N. Bacchetta[b], R. Bellazzini[a], D. Bon[c], A. Bondar[d], M. Bozzo[e], A. Brez[a], J.-M. Brom[f], J.-C. Caldero[c], J.-F. Clergeau[c], D. Contardo[c,*], M. French[g], A. Giraldo[b], G. Guillot[c], G. Hall[h], R. Hammarström[i], R. Haroutunian[c], L. Jones[g], T. Kachelhoffer[f], D. Kryn[c], M. Loreti[b], T. Ładziński[i], J.-C. Mabo[c], B. MacEvoy[h], M. Massai[a], M. Miguet[c], M. Millmore[h], A. Morelli[e], V. Nagaslaev[i,1], A. Pallares[f], F. Parodi[e], A. Peisert[i], S. Quian[f], F. Raffo[a], M. Raymond[h], M. Rebouillat[c], J.L. Riester[f], O. Runolfsson[i], R. Sachdeva[h], L. Shekhtman[i,1], G. Smadja[c], G. Spandre[a], M. Spezziga[a], A. Toropin[a], C. Vander Velde[j], P. Vanlaer[j], D. Vitè[h]

[a] *INFN, Pisa, Italy*
[b] *INFN, Padua, Italy*
[c] *IPN, Lyon, France*
[d] *BINP, Novosibirsk, Russian Federation*
[e] *INFN, Genova, Italy*
[f] *CRN, Strasbourg, France*
[g] *RAL, Didcot, United Kingdom*
[h] *IC, London, United Kingdom*
[i] *CERN , Switzerland*
[j] *ULB, Bruxelles, Belgium*

Received 1 June 1995

Abstract

During the beam test of a tracker prototype for the Compact Muon Solenoid detector proposed for the LHC, the time response of the Microstrip Gas Chambers was studied using different gases and chamber gaps. The subsequent efficiency to identify the bunch crossings at LHC is discussed for several algorithms used in the off-line signal processing of the data.

1. Introduction

Microstrip gas chambers have been chosen to equip the outer layers of the central tracker in the CMS experiment at LHC [1]. They provide the required resolution for momentum measurement and their high granularity allows to sustain particle rates of up to 10^5 Hz/mm^2 while maintaining the channel occupancy at a percent level. However, because of fluctuations in the charge collection, the signals generated in different bunch crossings, at the 40 MHz frequency of the LHC, can overlap in time and increase the overall occupancy of the detectors.

The goal of this work was to study this aspect of the MSGC response, referred to as the bunch crossing identification capability. Simulations of p–p events, taking into account the detector granularity, the CMS geometry and the 4 T magnetic field, show that the pileup of tracks generated in two bunch crossings should keep the occupancy at a tolerable level for efficient track reconstruction. The bunch crossing identification can thus be characterized by two parameters:

- the efficiency to identify the tracks produced in the bunch crossing associated with a trigger,
- the total number of tracks that will be identified at the trigger time, from any bunch crossing, normalized to the number of tracks produced in one bunch crossing. This ratio can be interpreted as the measure of bunch crossing pileup in the detector.

The values of these parameters will depend on the detector performance as well as on electronic signal

* Corresponding author.

[1] On leave of absence from BINP, Novosibirsk, Russian Federation.

SSDI 0168-9002(95)00633-8

processing. Both are discussed in this paper which is organised as follows:

The experimental set-up and the event selection are described in Section 2. In Sections 3 and 4 the average signal shapes, the mean amplitudes and the time resolutions measured with two drift distances and four different gas mixtures are presented.

In Section 5 the bunch crossing identification performance is compared for several algorithms employed in off-line signal processing of the data. A time measurement which is close to the ultimate capability of the detectors is presented as a reference to compare the performance of other algorithms based on a weighted sum of samples or a pulse shape selection. The baseline design for the read out of both the silicon and gas microstrip detectors in CMS is the RD20 scheme [2], which includes a fast amplifier and shaper, an analogue pipeline, a pulse shape processor and a multiplexer. The possibility to implement two of the tested algorithms in the pulse shape processor is discussed. Finally, bunch crossing identification performances are compared for detectors using different gas mixtures and chamber gaps.

2. Experimental set-up and event selection

The experimental set-up consisted of two microstrip gas chambers and two scintillator counters providing the trigger of the data acquisition. The microstrip gas chambers were manufactured[2] on the Schott glass Desag263 with aluminum strips of 250 mm length. The anode to anode distance was 200 μm and the anode and cathode strip widths were 9 μm and 74 μm respectively. The first chamber had a 2 mm drift distance while it was 3 mm in the second one. The general characteristics of these detectors are described in Ref. [3].

The detectors were read out with the Preshape32 chip, which is a 32 channel array of amplifiers fabricated using the MIETEC 1.5 μm CMOS process. It was developed by the RD20 collaboration, originally for use with silicon microstrip detectors at LHC [2,4]. Each channel consists of a charge sensitive preamplifier and a shaping amplifier. The shaping amplifier provides a *CR–RC* type pulse with a nominal peaking time of 45 ns, which is adjustable over a limited range. The gain of each channel, defined by the output load resistor, was 0.76 μV/e$^-$ for the value of 380 Ω used. The gain linearity is better than 1% for input signals up to 10^5 e$^-$, and better than 4% for signals up to 2×10^5 e$^-$. For a typical drain current of 440 μA in the input transistor, the equivalent noise charge is measured to be $500 + 50C_{ext}$ electrons, where C_{ext} (pF) is the total capacitance external to the amplifier. Four calibration inputs allow a test charge to be injected into all channels.

In all tests, the peaking time was set to 40 ns with the detectors connected, which contributed to an estimated load capacitance of ~12 pF. Each output from the chip was amplified in an external buffer[3] which drove the signals over 50 Ω coaxial cables. The buffers did not affect the pulse shape and the shortest possible cables, of 6 m length, were used to avoid further degradation.

A 4-channel sampling oscilloscope was used to digitize the signals from 4 adjacent strips in one of the chambers. An OR of 4 aligned strips in the other chamber in coincidence with the two scintillators provided the trigger. The jitter of the trigger was measured to be less than 2 ns. The signals were sampled at a frequency of 500 MHz over a time interval of 1 μs and stored on floppy disks. The set-up was installed in the H2 beam line at CERN and exposed to 300 GeV/c pions perpendicular to the detectors. Data were recorded for the following gas mixtures: Ar/DME (50/50), DME/CO_2 (80/20), DME/CF_4 (80/20) and pure DME. The voltages applied to the drift electrode and to the cathode strips are listed in Table 1. For safety of the detector operation, no attempts were made in this test to achieve the ultimate gas gains. The voltages were rather set to adjust the drift fields [3] around the same value of 10 kV/cm, with the exception of the DME/CF_4 mixture. In this case, it was 8.6 kV/cm since it had been observed in a preceding test that the gas gain was reduced at very high drift fields.

Because of a small misalignment between the two chambers not all the triggers were accompanied by a track in the chamber for which the pulses were registered. To ensure that signal processing was done on real track pulses, only those with an amplitude above three standard deviations of the electronic noise were considered. It was then required that the highest pulse above the threshold be measured on one of the two central strips. With these two conditions, the contamination by the noise was reduced to less than 0.02% of the total number of analysed events. The second selection criterion also ensures that when the

Table 1
Operating voltages and drift fields

Gas mixture	Gap [mm]	V_{drift} [V]	$V_{cathode}$ [V]	E_{drift} [kV/cm]
Ar/DME	2	2350	560	10
50/50%	3	3350	560	10
DME	2	2450	630	10
100%	3	3425	650	10
DME/CO_2	2	2450	640	10
80/20%	3	3425	660	10
DME/CF_4	2	2130	630	8.6
80/20%	3	3000	650	8.6

[2] Baumer Industrielle Messtechnik, Greifensee, Switzerland.

[3] Buf32 designed at IPN Lyon.

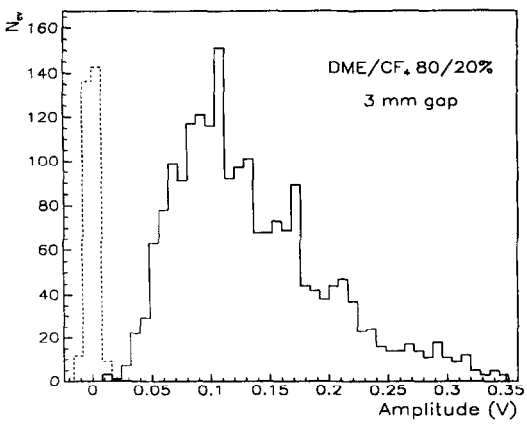

Fig. 1. Amplitude distribution of the noise (dashed line) and of the signal measured on the main strip (full line). The noise distribution is arbitrarily normalized.

charge generated by a track is collected on more than one strip all signals were analysed, if they crossed the threshold. The distribution of noise amplitudes was studied with samples recorded with a delayed trigger. The width of the distribution was 4.5 mV (rms) leading, with a threshold at 13.5 mV, to a final sample of about 2000 events for each experimental condition.

3. Amplitudes and pulse shapes

Using the selection criteria described above, all the gas mixtures and a 2 mm (3 mm) drift gave rise to about 70% (55%) of tracks with a single hit, with the rest of the events presenting two hits. In the following, the strip collecting the largest part of the signal is distinguished from the other strip, if present. They are respectively referred to as the main strip and the second strip.

Fig. 1 shows the noise amplitude distribution together with the amplitude distribution of the signal, measured on the main strip with the DME/CF_4 mixture and a 3 mm gap. As can be seen from the shape of the signal distribution, the detector was fully efficient at the chosen threshold. This was not the case with the Ar/DME mixture and to a lesser extent with the 2 mm gap for the other gas mixtures. This inefficiency is not of primary importance in the present analysis. In the following, it is mentioned whenever it introduces a bias in the data. For each set of experimental conditions, the mean amplitude ($\langle V \rangle$) measured at the pulse peak of the main strip is reported in Table 2. It was found to be 2 to 3 times larger than the observed value for the second strip, depending on the gas mixture and the chamber gap. This ratio is indicative of the diffusion of the carriers but it probably mainly depends on the signal to noise ratio, since the 3σ threshold applied increases the mean value of the second strip signal.

The largest mean amplitude of 135 mV, observed on the main strip, was obtained with the DME/CF_4 mixture and a 3 mm gap. A calibration of the full electronic chain, using the input test capacitance of 50 fF implemented in the Preshape32, allows an estimate of 42 000 e^- as the mean signal charge seen by the amplifier. It compares to an equivalent noise charge of 1400 e^-.

Comparing the data taken with the 2 mm and 3 mm gaps, the mean amplitude increases in proportion to the gas thickness, with the exception of the Ar/DME mixture for which the growth of the signal is smaller. In this case, as the amplitude distribution does not come completely above the threshold, the measured mean amplitudes are overestimated. The effect is larger when the signal is smaller,

Table 2
Mean amplitudes, ratios to the noise rms, event rates with signal on a single strip and time resolutions measured with various experimental conditions. The time distribution rms values are given (a) for the threshold crossing time (corrected according to the pulse amplitude, see text) and (b) for the pulse peak time

Gas mixture	Gap [mm]	$\langle V \rangle$ [mV]	$\frac{\langle V \rangle}{\text{noise}_{rms}}$	Events with 1 strip [%]	Time distribution rms [ns]	
					a	b
Ar/DME	2	44	10	72	14	17
50/50%	3	52	12	59	14	17
DME	2	61	14	69	11	14
100%	3	99	22	52	9	10
DME/CO_2	2	59	13	71	10	14
80/20%	3	94	21	50	8	10
DME/CF_4	2	84	19	69	8	10
80/20%	3	135	30	53	8	9

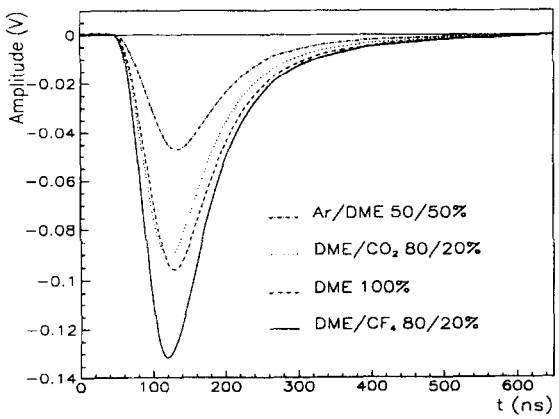

Fig. 2. Average of the registered pulses above the threshold.

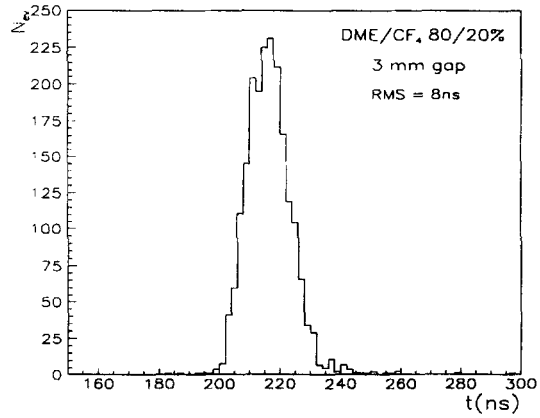

Fig. 3. Threshold crossing time distribution, after amplitude correction.

hence the non-proportionality between gas gap and mean amplitude.

Fig. 2 shows, for each gas mixture, the average shape ($\langle V(t)\rangle$) of all pulses above threshold, in the case of the 3 mm chamber gap and for the main strip. Because of the drift time of the carriers in the gas gap it exhibits a larger peaking time than the *CR–RC* impulse response of the amplifiers. The peaking time is 76 ns for the DME/CF_4 and DME/CO_2 mixtures and 83 ns in the case of pure DME and Ar/DME. This behaviour is qualitatively expected since the two first gas mixtures are known to give rise to a higher drift velocity [5].

4. Time resolutions

As described in Section 2, for each event 500 samples were recorded at a time interval of 2 ns. The simplest method of estimating the time resolution consists in measuring the time distribution of the first sample above threshold. However, smaller signals cross the threshold later than large amplitude pulses. To avoid this effect, the threshold crossing time was corrected according to the pulse amplitude.

Fig. 3 shows the final time distribution obtained with the DME/CF_4 gas mixture. The standard deviations for the various experimental conditions are summarized in Table 2 (a). The similar time resolutions observed with the 2 mm and 3 mm gaps indicate that the threshold is crossed when the first carriers reach an anode. The slightly worse time resolution with the 2 mm gap, in some cases, can be explained by a larger uncertainty on the time correction when the pulses are smaller. The observed time resolution for each gas is thus expected to depend on the mean number of primary electrons and on their drift velocity. The comparison of DME, DME/CO_2 and DME/CF_4 with a 3 mm gap shows that these gases have similar timing performance. In the case of pure DME, the effect of the smaller drift velocity (see Section 2) is compensated by the larger number of primary electrons. On the other hand, the worse time resolution observed with Ar/DME is compatible with the smaller primary ionisation and drift velocity expected with this gas [5].

The distributions of the time of the pulse peak were also studied. The standard deviations for the various experimental conditions are listed in Table 2 (b). A similar trend in the data, as with the threshold crossing time distributions, is observed. The results are only slightly worse with this method where the correction according to the pulse amplitude was not applied. A signal processing scheme using pulse samples around the peak of the pulse is thus expected to provide good bunch crossing identification as discussed in the following section.

5. Bunch crossing identification

In this section, the bunch crossing identification performance is compared for several algorithms used for off-line signal processing of the data. As described in the introduction, the procedure consists in determining the efficiency of the algorithm to identify the tracks corresponding to a bunch crossing associated with a trigger at LHC, together with the efficiency to identify the tracks produced in the surrounding bunch crossings, every 25 ns.

An algorithm is considered to be efficient when at least one of the signals generated in the MSGC has an amplitude higher than the threshold after processing. In this study, the threshold was chosen as three times the processed noise rms amplitude. It allows a direct comparison of the signal to noise ratio before and after the processing and was found to ensure an occupancy of the detectors, due to noise pulses, of less than 0.15% for all tested algorithms.

To simulate the situation at LHC, each set of events, corresponding to different experimental conditions, is considered a the total number of tracks produced in one

bunch crossing. The time of a trigger is defined so that the efficiency of signal processing is maximised. This optimised variable, ϵ, represents the efficiency to identify the tracks in the bunch crossing associated to the trigger. The efficiency to identify the tracks produced in preceding and subsequent bunch crossings is then estimated by applying the same procedure to intervals shifted by a multiple of the 25 ns LHC period. In the following the value of ϵ and the total efficiency to identify tracks, from any bunch crossing, are reported. This last number is referred to as the bunch crossing pileup, N_{bc} since, when multiplied by the number of tracks produced per bunch crossings it provides the total number of tracks that will be identified at the trigger time. In the tables of results, we have also reported the signal to noise ratio ($\langle V\rangle/\text{noise}_{rms}$), the relative amplitude resolution at the peak ($\Delta V/V$) and the event rates with signal on a single strip, obtained after processing.

The optimization of ϵ and N_{bc} relies on parameters specific to each processing algorithm. They are discussed in Sections 5.1 to 5.3, with the example of the data recorded with the DME/CF_4 mixture and a chamber gap of 3 mm. In Section 5.4, the performance of the different algorithms are compared and the possibility to implement some of them electronically is discussed. The results obtained with the various gases and chamber gaps are presented in the last section of this chapter.

5.1. Time and amplitude measurement

This method assumes that both signal amplitude and threshold crossing time are recorded. The threshold crossing time can thus be corrected for small amplitudes as described in Section 4. The efficiency, ϵ, and the bunch crossing pileup, N_{bc}, are then derived from the time distribution, shown in Fig. 3, considering the fractions of tracks in a given time window Δt centered on the mean value of the distributions. The results are summarized in Table 3. Although a time measurement is not foreseen in the readout scheme for CMS, this methods shows the ultimate performance of the detectors and will serve as a reference for other methods using less information.

Table 3
Efficiency and pileup of bunch crossings obtained within different time windows with the DME/CF_4 gas and a 3 mm chamber gap

Δt [ns]	ϵ [%]	Events with 1 strip [%]	N_{bc}
25	94.6	70	1.18
30	97.3	66	1.32
40	98.8	60	1.75
50	99.3	57	2.27
60	99.5	56	2.74

5.2. Weighted sum algorithm

The deconvolution of the *CR–RC* shaping of the amplifier is a weighted sum of several pulse samples first proposed by the RD20 collaboration to process the signal of silicon microstrip detectors [6]. In the ideal case of a δ-function input current pulse, the output of the deconvolution filter is confined to a single beam crossing interval. With three samples (V_t) the deconvoluted amplitude is:

$$V_{dec}(t_0) = W_1 W_{t0+2\Delta t} + W_2 V_{t0+\Delta t} + W_3 V_{t0} ,$$

where the weights W have the following expressions:

$$W_1 = (\tau/\Delta t)\exp(\Delta t/\tau - 1) ,$$

$$W_2 = -2(\tau/\Delta t)\exp(-1) ,$$

$$W_3 = (\tau/\Delta t)\exp(-\Delta t/\tau - 1) .$$

τ is the time constant of the *CR–RC* shaping and Δt is the sampling time interval.

As mentioned in Section 3, the fluctuations in the development of the MSGC signal modify the pulse shape as compared to the *CR–RC* response. The deconvolution is therefore not expected to be perfectly suited to this case. Nevertheless, it provides a method to choose weights and was applied here with τ and Δt as free parameters. The results are summarized in Table 4. They show that it will be difficult to approach the CMS requirements with suitable values of the parameters τ and Δt as the sample interval must be a multiple of the LHC period.

To avoid the implicit assumption on the pulse shape the deconvolution algorithm was used with weights adjusted to the data by an iterative procedure. One of the weights was fixed to 1 and the two others were varied successively until we reach the best compromise between ϵ and N_{bc}. This study was done using realistic time intervals of 25 ns and 50 ns between the three samples. The value of ϵ is optimised when the second sample is selected at the time of the maximum of the mean pulse shown in Fig. 2 and the best compromise between ϵ and N_{bc} was obtained with a 50 ns time interval. As can be seen in Table 4, this procedure leads to a better algorithm performance compared to simple deconvolution.

5.3. Shape selection algorithm

As an alternative to the weighted sum, methods based on a shape selection have been studied. The optimised value of ϵ was again obtained when selecting the second sample at the time of the mean pulse peak.

The first method is a comparison of the three sample amplitudes ($V(t)$) with their expected mean values ($\langle V(t)\rangle$) taken from Fig. 2. The deviation between the points is expressed by the following χ^2:

Table 4
Comparison of the bunch crossing identification with a weighted sum of three pulse samples, for weights given by the deconvolution or adjusted to the data with the DME/CF_4 gas and a 3 mm chamber gap

Deconvolution	Weight parameters	$\frac{\langle V\rangle}{\text{noise}_{rms}}$	$\frac{\Delta V}{V}$ [%]	ϵ [%]	Events with 1 strip [%]	N_{bc}
CR–RC	$\tau/\Delta t$ [ns]					
weights	90/24	9	26	93.1	85	1.79
	90/30	11	22	97.1	79	2.08
	70/30	12	20	98.0	79	2.30
	80/40	14	14	99.1	74	2.65
	70/50	19	10	99.6	66	3.22
Iterative	$W_1/W_2/W_3$					
weights	−0.7/1/−1	7	21	91.4	86	1.36
Δt = 50 ns	−0.6/1/−1	9	20	95.2	81	1.67
	−0.5/1/−1	11	16	97.0	81	1.87
	−0.4/1/−1	12	14	98.1	76	2.16
	0.0/1/−1	18	10	99.5	66	3.15

$$\chi^2 = (NV(t_0 - \Delta t) - \langle V(t_0 - \Delta t)\rangle)^2 + (NV(t_0 + \Delta t) - \langle V(t_0 + \Delta t)\rangle)^2,$$

where, $N = \langle V(t_0)\rangle / V(t_0)$, is a normalization factor taken at the time t_0 of the mean pulse peak. To estimate the efficiency, the amplitude of the second sample was preserved for a χ^2 value below a given threshold and set to 0 otherwise. The best compromise between the values of ϵ and N_{bc} was obtained with a time interval of 50 ns between the samples. The results are summarized in Table 5 for different values of the threshold (χ^2_{th}).

The second method is a simple comparison of the three samples to identify if the pulse peak is the second sample [7]. Its amplitude is preserved if it is above the two others and set to 0 otherwise. In this case, the two time intervals between the samples ($\Delta t_{12}, \Delta t_{23}$) are the free parameters. The results, presented in Table 5, show a good compromise between ϵ and N_{bc} with asymetric time intervals between the samples, but still respecting the LHC period. This behaviour is not surprising since one can expect the method to be optimised when the amplitude difference between the second sample (pulse peak) and the two others is maximum. It indicates that a symetric pulse shaping with a smaller time constant could yield better results. This comment can apply to the weighted sum algorithm for which the best choice of the pulse samples was also at the time of the mean pulse peak and around. On the other hand, such a shaping will probably increase the electronic

Table 5
Comparison of the bunch crossing identification for a shape selection with a χ^2 method or an identification of the pulse peak for the DME/CF_4 gas and a 3 mm chamber gap

Shape selection	Parameters	$\frac{\langle V\rangle}{\text{noise}_{rms}}$	$\frac{\Delta V}{V}$ [%]	ϵ [%]	Tracks with 1 strip [%]	N_{bc}
χ^2	χ^2_{th}					
Δt = 50 ns	0.001	27	2	92.3	82	1.09
	0.002	29	3	97.5	73	1.40
	0.003	29	3	98.7	69	1.66
	0.004	29	4	99.0	65	1.89
	0.005	29	4	99.1	64	2.09
Peak	$\Delta t_{12}/\Delta t_{23}$ [*ns*]					
finding	24/24	26	2	91.5	75	1.15
	30/30	28	2	95.5	71	1.32
	40/40	29	3	98.6	63	1.78
	48/48	29	3	99.2	62	2.18
	24/48	28	3	97.4	67	1.45
	24/72	28	5	98.9	64	1.77

noise as compared to the present *CR–RC* shaping. The final choice will thus be mainly determined by the achieved signal to noise ratio.

5.4. Comparison of the different algorithms

The results of the different signal processing methods, listed in the preceding tables for the DME/CF_4 mixture with a 3 mm gap, are drawn together in Fig. 4. It can be seen that the two shape selections perform almost as well as the time measurement. One reason is that the time resolution at the pulse maximum is close to the ultimate value measured at the threshold, as explained in Section 4. The second reason, is that the signal to noise ratio, at three standard deviations (see Tables 2, 4 and 5), is almost preserved by these algorithms, which is not the case with the weighted sum method where it is reduced by 30 to 70%, depending on the choice of the weights. The shape selections are thus more efficient to identify the smaller signals and provide better results. As another consequence, the amplitude resolution is better and the rate of events with a single signal is also closer to its value before the signal processing. When the shape selections are compared to the weighted sum algorithms they will yield better spatial resolution if the position of a track is determined by a center of gravity method and higher efficiency to measure the obliquely incident tracks for which the signal can be shared on a large number of strips.

Although good performance can be realised using several signal processing strategies, an important practical issue is the ease with which an algorithm can be implemented in an electronic circuit. At LHC this filtering operation is carried out on the detector in the form of a custom designed part of the front end ASIC (application specific integrated circuit). Power consumption and chip size, as well as performance, are important issues.

The deconvolution method has been demonstrated as a working circuit using a switched capacitor design [6] and

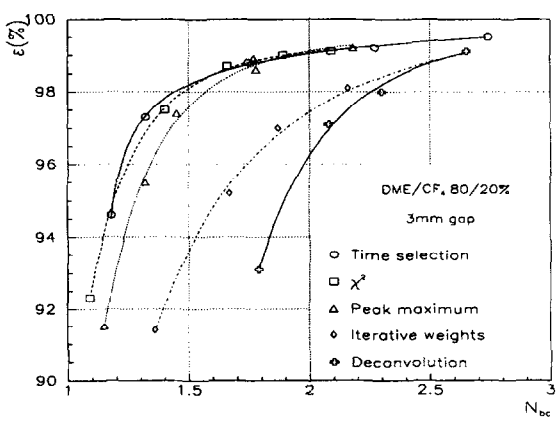

Fig. 4. Comparison of the different signal processings for the DME/CF_4 mixture with a 3 mm gap.

variants, such as the use of four samples instead of three, can be handled without difficulty. The selection of weights adjusted to the specific pulse shape of the MSGC signal is also a variant of the deconvolution filter which requires only minor modifications. However, peak finding algorithms have not so far been used and raise some questions. A possible simple circuit schematic is shown in Fig. 5. A logical AND of two comparison of the three input levels of the signal pulse is used to define the output; V_{out} is set low in case of no peak. Both comparators are however assumed to have identical thresholds, with no offsets. In practice, the offsets will give rise to some bias at the output of the system which will mainly affect small signals and noise peaks. This may create difficulties in monitoring the operation of the system which requires careful study.

5.5. Comparison of the bunch crossing identification with the different gases and chamber gaps

A comparison of the bunch crossing identification performance with different gases and chamber gaps is made in Fig. 6, for the time measurement, the pulse peak identification and the weighted sum with iterative weights.

The best results are obtained with the DME/CF_4 mixture. They are similar for the 2 mm or 3 mm gap with the time measurement, as expected since the time resolutions are the same for both drift distances. On the other hand, with the weighted sum or the pulse peak selection, the results are better with the 3 mm gap, showing that these algorithms are sensitive to the initial mean signal to noise ratio (before the signal processing) rather than to the timing properties of the gas. The DME and DME/CO_2 mixtures give similar results while the efficiency is rather low with Ar/DME. It has to be noted, that the reported efficiency is the algorithm efficiency estimated from a sample of tracks having at least one signal above three times the noise rms before the signal processing. With the Ar/DME mixture, as it was mentioned in Section 3, not all the track signals reach this threshold. The algorithm efficiency is thus higher than the real efficiency in this case. This is also true to some extent for the other data with the 2 mm gap.

The conclusion is that, with the conservative operating conditions used in this test, the signal to noise ratio was the

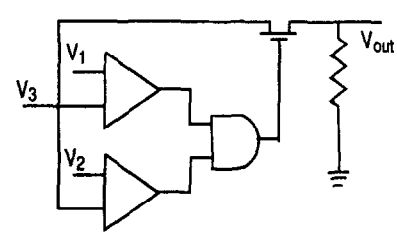

Fig. 5. Schematic of a possible circuit for peak maximum identification.

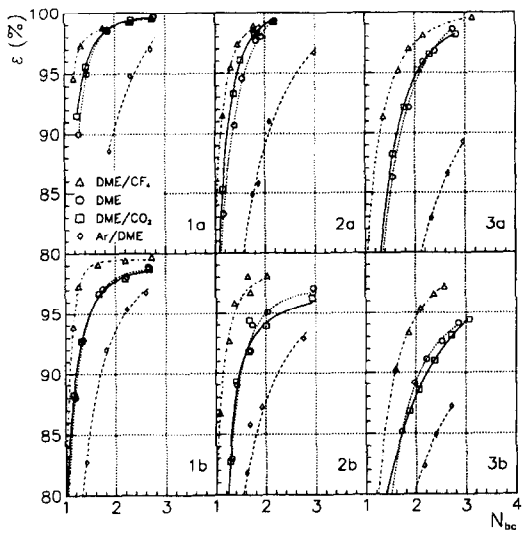

Fig. 6. ϵ versus N_{bc}, (1) for the time measurement, (2) for the pulse peak identification and (3) for the weighted sum. (a) With a 3 mm gap and (b) with 2 mm.

most important parameter for optimal signal processing as compared to the proper timing properties of the different gases. The time resolutions presented in Section 4 indicate that if the same signal size as with the DME/CF_4 mixture can be produced with DME or DME/CO_2 a similar performance of the bunch crossing identification can be expected with these gases. However, it will probably be more difficult to reach the same performances with Ar/DME, even at a same signal level, since it appears to have intrinsically worse timing properties.

6. Conclusions

The bunch crossing identification at LHC was studied with minimum ionizing particles crossing a perpendicular microstrip gas chamber equipped with RD20 amplifiers. With a DME/CF_4 (80/20) gas mixture and a chamber gap of 3 mm, a weighted sum or a pulse peak identification using three pulse samples has been shown to achieve 96% track finding efficiency with a bunch crossing pileup of respectively 1.8 and 1.4, compatible with the requirements for the CMS central detector.

The signal to noise ratio after signal processing is larger with the pulse peak identification. This algorithm is therefore more efficient to identify the smaller signals as will be the case with angled tracks. The difference in performance between the two algorithms will probably be reduced with higher MSGC signals but this has to be tested in realistic conditions. Although the pulse shaping of the RD20 amplifier seems adequate, it is not excluded that it could be optimized to improve the performance when using samples selected around the pulse peak.

While the weighted sum has already been implemented electronically, this possibility for a pulse peak selection is currently being investigated.

When comparing the different gas mixtures and chamber gaps, it appears that the results depend mainly on the signal amplitude. Further tests will be needed to determine the best performance achievable with different gases in stable long term operation of the detectors. The final choice of a chamber gap will depend on a compromise between the efficiency and the occupancy especially when including the effect of slant tracks.

Acknowledgements

We would like to thank the team of O. Runolfsson for their help in building the readout electronics and in the installation of our set-up in the beam area. We thank Mrs. M. Plage and E. Gimenez from CRN Strasbourg for wiring the low voltage regulators, and M. Goyot from IPN Lyon for help in the hybrid design.

References

[1] The Compact Muon Solenoid Technical Proposal, CERN/LHCC 9438 LHCC/pp1 (1994).
[2] RD20 Status Report, CERN/DRDC 94.39 (1994).
[3] F. Angelini et al., Nucl. Instr. and Meth. A 343 (1994) 441.
[4] M. Raymond and L. Jones, Preshape32 User manual, RD20 internal technical note.
[5] M. Geijsberts et al., Nucl. Instr. and Meth. A 313 (1992) 377.
[6] N. Bingefors et al., Nucl. Instr. and Meth. A 326 (1993) 112; M. Millmore et al., IC/HEP/95/3, submitted to Nucl. Instr. and Meth.
[7] J.F. Clergeau et al., Nucl. Instr. and Meth. A 355 (1995) 359.